Catalytically Active Gold Clusters with Atomic Precision for Noninvasive Early Intervention of Neurotrauma

Yunguang Zhang
Xi'an University of Posts and Telecommunications
Si Sun
Tianjin University
Haile Liu
Tianjin University
Qinjuan Ren
Tianjin University
Wenting Hao
Tianjin University
Qi Xin
Tianjin University
Jiangang Xu
Xi'an University of Posts and Telecommunications
Hao Wang
Tianjin University
Xiao-Dong Zhang (xiaodongzhang@tju.edu.cn)
Tianjin University

Research

Keywords: Gold nanoclusters, Catalytic activity, Traumatic brain injury, Noninvasive administration

Posted Date: June 18th, 2021

DOI: https://doi.org/10.21203/rs.3.rs-624731/v1

Abstract

Background

Neurotrauma is a head or spine injury caused by external forces. It is associated with oxidative stress, caused by the overproduction of peroxides and superoxides, and that can induce wound infection and trigger a serial of immunological reactions. The emerging catalysts have shown great potential for the treatment of brain injury and inhabiting neurogenic inflammation, but are limited to biosafety issues and delivery efficiency.

Results

Herein, we propose the noninvasive delivery route to brain trauma by employing highly active gold clusters with enzyme-like activity for achieving the early intervention. The ultrasmall gold clusters with unique size distribution show excellent catalytic activity with 10 times decomposition rate to H_2O_2. *In vitro* experiment shows the gold clusters can decrease the excessive $O_2^{\bullet-}$ and H_2O_2 compared with untreated cells. *In vivo* experiment shows gold clusters accelerate the wound healing of brain trauma and decrease the peroxide and superoxide of brain tissue. The western blot shows noninvasive treatment can decrease the inflammatory factors via inhibiting the activation of astrocytes and microglia.

Conclusions

Present work shows noninvasive treatment is a promising route for early intervention of brain trauma.

Background

Traumatic brain injury (TBI) is a serious public health concern leading to death and disability with high morbility globally [1–3] and causes economic burden [4–6]. Despite the primary insults, the TBI can cause secondary injury which is highly related with oxidative stress and will lead to chronic neurodegenerative diseases [1, 7–9]. Further, free radicals of reactive oxygen species (ROS) like hydroxyl radical ($OH^{\bullet}$), superoxide anion radicals($O_2^{\bullet-}$), hydrogen peroxide (H_2O_2) and reactive nitrogen species (RNS) such as nitric oxide radicals ($NO^{\bullet}$) and peroxynitrite ($ONOO^-$), which can oxidatively impair the biomacromolecules and play a crucial role in TBI [1, 7, 8, 10, 11]. Thus, the elimination of reactive oxygen and nitrogen species (RONS) is vital for the treatment of TBI, and antioxidative biocatalysts that can catalytically scavenge the RONS are promising in TBI treatment. Particularly, catalytic nanoclusters acting as enzymes like catalase (CAT), superoxide dismutase (SOD), peroxidase (POD) and glutathione peroxidase (GPx) with high catalytic performance and good stability are being developed constantly and have shown great potential for the treatment and diagnosis of TBI [12–20].

To date, several nanozymatic biocatalysts were exploited for the treatment of TBI. For instance, carbogenic and gold-based nanozymes exhibited exceeding activity against oxidative stress and neuroinflammation promising their use in TBI treatment [13, 21–24]. Nanoclusters composed of metals, metallic oxide and alloys like Pt, Pd, Cr, V and Ce possessing high enzymatic activities were developed for TBI treatment [12, 14, 15, 18, 25–27]. Especially, the ceria nanozymes exhibited enzymatic activities like SOD and CAT on scavenging RONS via redox cycle between Ce^{4+} and Ce^{3+} [12, 18, 25, 28]. Gold nanoclusters can simulate SOD, CAT and GPx enzymes displaying compelling effects in TBI treatment with superb antioxidant capacities [29–33]. Besides, diagnosis and monitoring methods based on nanotechnologies especially activable nanoprobes are being developed for TBI [34–36], and technologies like atom engineering, surface modification, and size modulation were employed to promote the activity and utilization of nanozymatic biocatalysts [30–32, 37–44]. To achieve rapid and painless treatment, noninvasive diagnosis and stimulation for TBI are worth considering to promote recovery and minimize disability [45, 46]. At present, multiple noninvasive methods for TBI modulation were developed and noninvasive administration of therapeutic nanozyme shows a promising prospect [12, 15, 47].

Herein, we investigated the catalytic activity and therapeutic outcome of gold nanoclusters on TBI with noninvasive intervention. Electrochemical assay unraveled their high catalytic activities toward hydrogen evolution reaction (HER) and oxygen evolution reaction (OER), and further revealed their excellent activity toward the reduction of O_2 and H_2O_2. The good activity of the gold nanoclusters on ROS scavenging *in vitro* and *in vivo* was observed. Furthermore, noninvasive administration of the gold nanoclusters distinctly improved the wound healing on TBI mice and Morris water maze tests further confirmed significant recovery on learning ability and spatial memory with $Au_{24}Cu_1$ and $Au_{24}Cd_1$ treatment. E*x vivo* assay further confirmed the ability of gold nanoclusters on mitigating oxidative stress and inhibiting neuroinflammation. Together with the results of acceptable biocompatibility, gold nanoclusters showed promising potential as noninvasive therapeutics against TBI.

Results And Discussion

Figure 1a illustrated the effects of MPA-protected Au_{25}, $Au_{24}Cu_1$ and $Au_{24}Cd_1$ nanoclusters in brain trauma *via* catalytic systems. TEM images illustrated the homogenous distribution of the nanoclusters at about 2 nm (Fig. 1b, 1c), similar with L-NIBC-coated gold nanoclusters [48]. The hydrodynamic sizes for Au_{25}, $Au_{24}Cd_1$ and $Au_{24}Cu_1$ determined by dynamic light scattering (DLS) were 1.98, 1.92 and 2.58 nm respectively, which was larger than the statistical diameter of TEM. The size changed negligibly after incubation in water for 24 and 48 h, revealing the favorable stability of the nanoclusters (Fig. 1d, 1e). In addition, the zeta potentials of all nanoclusters were around − 35 mV (Fig. 1f), consistent with our previous work [29, 49]. These results indicate the ultrasmall size and good colloid stability of nanoclusters, showing the potential in biological applications.

To evaluate the electrocatalytic activities of the Au_{25}, $Au_{24}Cu_1$ and $Au_{24}Cd_1$ nanoclusters, we employed a standard three-electrode system to conduct the electrocatalytic HER and OER activities toward HER and

OER [50–52]. Figure 2a shows cyclic voltammetry (CV) curves of glassy carbon (GC) electrodes modified with as prepared Au_{25}, $Au_{24}Cu_1$ and $Au_{24}Cd_1$ nanoclusters. Compared with a blank GC electrode, nanoclusters achieve larger negative current density toward HER (Fig. 2a), which were further verified by linear sweep voltammetry (LSV) measurement (Fig. 2b). In comparison, the current density of $Au_{24}Cu_1$ nanoclusters at the potential of − 0.4585 V as described in histograms (Fig. 2c) demonstrated a higher efficiency in catalysis, showing superiority on HER activity. OER shows similar results with HER that all nanoclusters improved the performance of the electrochemical reaction (Fig. 2d-2f). However, the $Au_{24}Cd_1$ nanocluster was more efficient than the $Au_{24}Cu_1$ nanocluster toward OER that the $Au_{24}Cd_1$ haves the lowest current onset on CV curves at 1.3 V, followed by $Au_{24}Cu_1$ and Au_{25}, which is a little different from the results of HER.

We also evaluated the *in vitro* catalytic activities of Au_{25}, $Au_{24}Cu_1$ and $Au_{24}Cd_1$ nanoclusters in H_2O_2 reduction and oxygen reduction reaction (ORR) at the scan rate of 10 mV s^{-1} [53, 54]. Figure 3a demonstrated that all nanoclusters could enhance the electrocatalytic activity for reduction of O_2 while $Au_{24}Cu_1$ nanoclusters show the current density of -1.48 mA/cm^{-2} at the potential of -0.8 V, indicating the best activity of $Au_{24}Cu_1$ nanoclusters for ORR among all nanoclusters. The results were further verified by LSV measurement (Fig. 3b) and the current density of nanoclusters at -0.8 V was compared in Fig. 3c. For the reduction of H_2O_2, only imperceptible reduction current was observed in the presence of H_2O_2 on the GC electrode, consistent with previous works [53]. Compared with the GC electrode at -0.8 V, $Au_{24}Cu_1$ nanoclusters showed the current of -1.74 mA/cm^{-2}, while $Au_{24}Cd_1$ nanoclusters showed the current of -1.56 mA/cm^{-2} (Fig. 3d, 3e), indicating excellent catalytic activities toward reduction of H_2O_2. Figure 3c and 3f demonstrated the improvement of all nanoclusters on O_2 and H_2O_2 reduction. $Au_{24}Cu_1$ showed the predominance toward both reactions, and $Au_{24}Cd_1$ and Au_{25} followed closely toward H_2O_2 and O_2 reduction respectively. The electrochemical assessments of nanoclusters substantiated their remarkable *in vitro* catalytic activities in H_2O_2 and O_2 reduction reactions, inspiring us to investigate their biological responses in cells and brain-injured mice.

As the nanoclusters exhibited extraordinary catalytic activities which set the foundation for their use in ROS-related diseases, we conducted a biological inspection to evaluate their activities *in vitro* and *in vivo*. With the combination of our previous work [29], we concluded that the $Au_{24}Cd_1$ and $Au_{24}Cu_1$ nanoclusters exhibited selectivity on ROS and RNS and showed selective SOD-like and CAT-like activities, which can reduce the oxidative stress induced by brain injury and perform the therapeutic effect (Fig. 4a). Additionally, the $Au_{24}Cd_1$ and $Au_{24}Cu_1$ nanoclusters presented favorable biocompatibility and metabolic properties, which benefits their use *in vivo* [29].

To investigate the biological activity of nanoclusters, imaging of H_2O_2-treated neuron cells was performed with or without Au_{25}, $Au_{24}Cd_1$ and $Au_{24}Cu_1$ nanoclusters (Fig. 4b). The H_2O_2 significantly elevated the signals, indicating the presence of the excessive amount of ROS [55], especially $O_2^{\bullet-}$. All clusterzymes can decrease the $O_2^{\bullet-}$ signals, while $Au_{24}Cd_1$ shows the best clearance efficiency.

Meanwhile, The H_2O_2 treatment enormously increases the ROS signal, and $Au_{24}Cu_1$ displays better clearance capability than Au_{25} and $Au_{24}Cd_1$, suggesting higher selectivity for ROS. The relative quantification of oxidative stress toward fluorescent images was shown in Fig. 4d and 4e, further confirming the remarkable biological catalytic activity and laying the groundwork for *in vivo* utilization. In addition, H_2O_2 induces decreases in cell viability (~78%) due to oxidative stress and inflammation [56], while Au_{25}, $Au_{24}Cd_1$ and $Au_{24}Cu_1$ nanoclusters can rescue the decreases induced by H_2O_2 back to 90%, indicative of the good potential of nanoclusters to rescue the lethality induced by H_2O_2 (Fig. 4c). All the *in vitro* results manifest good catalytic activities of $Au_{24}Cd_1$ and $Au_{24}Cu_1$ nanoclusters on ROS scavenging, revealing their potential as biocatalysts and suggesting further investigation on animal models.

To investigate the usability of the nanoclusters against TBI, we performed craniotomy and Morris water maze tests as well as the assessment of oxidative stress and inflammation level in brain tissues of TBI mice. Figure 5a and 5b show the wound healing processes over time of TBI mice with or without treatment of nanoclusters. Compared with the TBI group, all nanoclusters promoted the healing progress among which the $Au_{24}Cd_1$ presented the best healing effect followed by $Au_{24}Cu_1$, demonstrating the therapeutic effect of the nanoclusters especially the $Au_{24}Cd_1$ and $Au_{24}Cu_1$. In addition, we evaluated the oxidative stress-related indicators, including SOD, GSH/GSSG, MDA, and H_2O_2 in TBI mice after nanoclusters treatment [33, 57].TBI can consume lots of SOD and GSH, leading to the decrease of SOD and GSH activity and the increase of MDA and H_2O_2 amount (Fig. 5c-f). The presence of over-excessive MDA H_2O_2 and GSSG indicates severe oxidative stress in TBI mice. After nanoclusters treatment, the activity of SOD and GSH/GSSG is increased while that of the oxidative-stress related byproducts MDA and H_2O_2 is decreased. Therefore, nanoclusters can intervene in TBI treatment by reducing oxidative stress.

The behavior tests were conducted to evaluate the spatial learning and memory abilities by Morris water maze (Fig. 6). Figure 6b showed the path of the mice searching the platform which presented the significant difference between the mice with and without administration of $Au_{24}Cu_1$ or $Au_{24}Cd_1$. Mice in the control group could quickly locate and land on the platform, while the mice in the TBI group could not locate the exact position of the platform in a short time. The mice with noninvasive administration of gold nanoclusters could find the platform after a short period and dopped gold clusters revealed better results than Au_{25}, indicating the enhancement of efficiency by Cu and Cd single-atom substitution. During 13–17 and 26–30 days after treatment, compared with the TBI group, both the total distance and the latency to the target site were reduced significantly after $Au_{24}Cu_1$ and $Au_{24}Cd_1$ nanoclusters treatment (Fig. 6c, 6d), suggesting that nanoclusters could improve the learning ability of injured mice. On days 17 and 30, the number of platform crossings was significantly increased close to the result of the control group and the average distance to the platform was reduced significantly in the groups of $Au_{24}Cu_1$ and $Au_{24}Cd_1$. All the indicators of the behavioral test demonstrated that the neuronal cognition of mice treated with $Au_{24}Cu_1$ and $Au_{24}Cd_1$ nanoclusters is improved, and the spatial learning and memory

abilities of treated mice are close to healthy mice, further confirming that nanoclusters could improve the spatial learning and memory abilities.

The effects of nanoclusters on neuroinflammation were examined for further verification of the therapeutic effect. Figure 7a illustrated the TBI-associated inflammatory responses and modulation of the nanoclusters [1, 8]. The IL-1β, IL-6 and TNF-α were upregulated by TBI, revealing strong local inflammation. $Au_{24}Cd_1$ exhibited exceptional efficiency to downregulate all three inflammatory factors, indicating its strong anti-neuroinflammation effect *in vivo*. $Au_{24}Cu_1$ can significantly downregulate the overexpression of TNF-α, presenting superior efficacy over $Au_{24}Cd_1$. In comparison, Au_{25} only showed minor downregulation toward the three inflammatory factors, as manifested in the catalytic activity induced by substitution of Cu and Cd (Fig. 7b, 7c). In addition, the ELISA further verified the immunoblot results that $Au_{24}Cd_1$ and $Au_{24}Cu_1$ are superior to Au_{25} on inhibiting the inflammatory factors in brain tissues including IL-1β, IL-6, and TNF-α (Fig. 7d-7f). Figure 7g quantitatively analyzed the positive cell numbers in injured cortex treated with H_2O_2 with or without nanocluster and presented the significant anti-inflammation effect of $Au_{24}Cd_1$ and $Au_{24}Cu_1$. Additionally, the immunohistochemical assay illustrated the conspicuous effect of $Au_{24}Cd_1$ and $Au_{24}Cu_1$ against IL-6 (Fig. 7h). Furthermore, significant differences on the pathological slices can be seen that the TBI group exhibited swelling of nerve cells and obvious infiltration of inflammatory cells; while the groups treated with nanoclusters especially the $Au_{24}Cd_1$ and $Au_{24}Cu_1$ recovered to almost normal (Fig. 7i). These results demonstrated that the nanoclusters especially $Au_{24}Cd_1$ and $Au_{24}Cu_1$ can accelerate the wound healing of traumatically injured brain by inhibiting the inflammatory factors.

Microglia and astrocytes are the key cellular mediators of TBI and mice after TBI can activate microglia and astrocytes [1]. As shown in Fig. 8a, lots of astrocytes are produced and activated after TBI along with inflammatory cytokines, indicating strong local inflammation. However, $Au_{24}Cd_1$ and $Au_{24}Cu_1$ nanoclusters can remarkably decrease the overexpression of IL-1β and IL-6, in addition to inhibiting astrocyte activation. The relative quantification further exhibited the significant effect of $Au_{24}Cd_1$ and $Au_{24}Cu_1$ nanoclusters (Fig. 8b). $Au_{24}Cd_1$ can alleviate IL-1β and IL-6 associated immune response, while $Au_{24}Cu_1$ has a better effect on reducing TNF-α, indicating their catalytic selectivity and potential selectivity towards the treatment of neuroinflammation. The *ex vivo* investigation further verified the catalytic activity of $Au_{24}Cd_1$ and $Au_{24}Cu_1$ against neuroinflammation and manifested the significant effect of promoting the healing of TBI.

The present work demonstrated the high catalytic activity of $Au_{24}Cd_1$ and $Au_{24}Cu_1$ nanoclusters and their availability as TBI therapeutics. More importantly, our investigation revealed that noninvasive administration is a potent strategy for TBI treatment since it can directly and rapidly release the biocatalysts into the damaged area, eliminating the RNOS and inhibiting subsequent neuroinflammation [15, 29, 58, 59]. Necessarily, exploiting new biocatalysts with high catalytic activities and favorable biocompatibility and developing new delivery modes for the biocatalysts for the noninvasive intervention of TBI will be a constant challenge in this field [15, 45]. As more biocatalysts with distinguished catalytic

activities against oxidative stress are being developed [20, 60], there will be more potential therapeutics in the use of noninvasive intervention against TBI.

Conclusions

We reported that noninvasive early intervention of gold nanoclusters gave a better outcome for neurotrauma and should be a powerful strategy for the cure of TBI. The nanoclusters we reported here showed high catalytic activities toward water splitting and reduction of O_2 and H_2O_2, which animated their use in oxidative stress-related diseases especially TBI. By employing the catalytical nanoclusters, we successfully demonstrated the importance of oxidative stress in the genesis and development of TBI and the exceptional effect of early intervention using enzymatic biocatalysts for the treatment. The biological results found that $Au_{24}Cd_1$ preferentially decreases IL-1β and IL-6, while $Au_{24}Cu_1$ shows the tendency to decrease TNF-α, indicating their different selectivity for alleviating neuroinflammation. Animal models illustrated their favorable effects against TBI after noninvasive administration. In conclusion, our work showed the great potential of noninvasive early intervention for the treatment of TBI with enzymatic biocatalysts.

Materials And Methods

Materials and reagents

All chemicals and reagents were purchased from commercial sources and used without further purification. Gold chloride ($HAuCl_4{\cdot}3H_2O$) was purchased from Sigma-Aldrich. Copper nitrate ($Cu(NO_3)_2$), Cadmium nitrate ($Cd(NO_3)_2$), 3-Mercaptopropionic acid (MPA), Sodium borohydride ($NaBH_4$), Sodium hydroxide (NaOH), were purchased from Aladdin. Ultrapure water (18.2 MΩ*cm) was used for all the experiments. Kits and fluorescent probes were purchased from commercial sources and used as per the instructions.

Materials preparation, characterization and catalytic activities

The MPA-protected Au_{25}, $Au_{24}Cu_1$ and $Au_{24}Cd_1$ nanoclusters were prepared as per the previous report [29, 61, 62]. Briefly, $HAuCl_4$ (aqueous, 20 mM, 0.25 mL) and MPA (aqueous, 5 mM, 2 mL) were added to water (2.35 mL) and stirred for 5 min at room temperature. Then, NaOH solution (aqueous, 1 M, 0.3 mL) was added to the reaction mixture, followed by the addition of 0.1 mL of $NaBH_4$ (43 mg of $NaBH_4$ powder in 10 mL of 0.2 M NaOH solution). $Au_{25}MPA_{18}$ was collected after the final reaction mixture stirred at room temperature for 3 hours in the dark and aged at 4 °C for 12 hours. The $Au_{24}Cu_1$ and $Au_{24}Cd_1$ were synthesized based on the same method, except the Au atoms in $HAuCl_4$ (20 mM, 0.25 mL) were replaced by various nitrate metal ions (Cu^{2+}, Cd^{2+}) at a 4% molar ratio. Ultrafiltration tubes of 3 K and 10 K at 3500 rpm/min were used for ultrafiltration to remove smaller organic ligands and larger-sized clusters, and lyophilization was used to collect the purified product for further test and investigation.

A JEM-2100F electron microscope (JEOL, Japan) was employed to acquire transmission electron microscopic (TEM) images. A Malvern Zetasizer Nano ZS90 (UK) was employed to measure dynamic light scattering (DLS) to test the hydrodynamic size and determine the zeta potential of nanoclusters.

The nanoclusters were deposited onto the surface of glassy carbon (GC) electrodes for electrochemical assay [14, 42]. Briefly, as-prepared MPA-protected Au_{25}, $Au_{24}Cu_1$ and $Au_{24}Cd_1$ nanoclusters (20 μL, 0.5 mg/mL) were deposited onto the surface of GC electrodes and dried naturally, then Nafion solution (3 μL) was dropped onto the surface of GC electrodes and dried, the modified electrodes were used for catalytic activity tests.

Cyclic Voltammetry (CV) and Linear Sweep Voltammetry (LSV) measurements were taken (scan rate: HER, 10 mV s^{-1}; OER, 100 mV s^{-1} electrochemical analyzer, CHI660D, Shanghai) to evaluate the performance of the nanoclusters modified electrodes for HER and OER. HER was carried out in 0.5 M H_2SO_4, and a graphite rod and a saturated calomel electrode were used as the counter electrode and reference electrode, respectively. OER was carried out in 1 M KOH, and a platinum wire and an Ag/AgCl electrode were used as the counter electrode and reference electrode, respectively.

CV and LSV measurements were taken (scan rate, 50 mV s^{-1}, electrochemical analyzer, CHI660D, Shanghai) to evaluate the catalytic activities for O_2 and H_2O_2 reduction. A three-electrode cell was adopted for both O_2 and H_2O_2 reduction, a platinum wire and a saturated calomel electrode were used as the counter electrode and reference electrode, respectively. Oxygen reduction reaction (ORR) was carried out in O_2-saturated in 0.01 M PBS (pH 7.4), and the H_2O_2 reduction was performed in the presence of 9.8 mM H_2O_2 in N_2-saturated 0.01 M PBS (pH 7.4).

In vitro evaluation of the catalytic activities

Mouse hippocampal neuronal cell line (HT22) was used in all the cellular experiments. Cells were seeded into the 96-well plates and grew in Dulbecco's modified Eagle's medium (DMEM) at 37°C with 5% CO_2. After being stimulated with 100 μM H_2O_2 for 6 hours, the culture medium was replaced by Au_{25}, $Au_{24}Cu_1$ and $Au_{24}Cd_1$ dissolved in the DMEM at different doses, and then cells were incubated for another 24 hours. Cell survival was analyzed using MTT (3-(4,5-dimethyl-2-thiazol)-2,5-diphenyl-2H tetrazolium bromide, Beyotime). HT22 cells (1 x 10^5 cells per well) were seeded in 6-well plates for 12 hours and stimulated with 100 μM H_2O_2 for 6 hours before being treated with the nanoclusters (12 ng/μL). Fluorescent staining was carried out to evaluate the intracellular oxidative stress levels with different probes such as DHE for $O_2^{\bullet-}$ and DCFH-DA for ROS, and cell images were captured by a fluorescence microscope.

In vivo treatment and behavioral experiment

TBI models: C57BL/6 mice at 21–23 g were employed to establish TBI models using an electromagnetically CCI injury device (eCCI-6.3, Custom Design & Fabrication, Inc), with an impactor of 5

m/s velocity, 0.61 mm depth, 150 ms duration, and 20° angle of dura mater on the vertical axis. The mice were divided into control, TBI, TBI + Au_{25}, TBI + $Au_{24}Cu_1$, and TBI + $Au_{24}Cd_1$ group (n = 15) randomly. All mice were anesthetized with 10 % chloral hydrate (10 mg/kg) and the scalp was cut before placed on the stereotaxic frame. The craniotomy was carried out by drilling the skull in a circle of 2 mm in diameter. The scalp was sewn together carefully, and the nanoclusters were added to the wound of TBI mice at a concentration of 50 mg/kg. The healing process was recorded photographically and the wound remaining was calculated after treatment.

Oxidative stress level: Brain tissues were taken out on days 7 and 14 post-treatment, then homogenized in 0.9 % physiological saline and analyzed for SOD, GSH/GSSG, MDA, and H_2O_2 using commercially available kits. All testing methods are carried out as per the instructions (Beyotime).

Morris water maze tests: Morris water maze (MWM) was conducted on days 13–17 and 26–30 post-treatment as described in the previously reported literature [12, 63, 64]. Briefly, the water maze was divided into four quadrants, and the platform was set in the center of quadrant I. Before spatial learning, visual discrimination learning was performed to determine whether the vision of mice was normal. In this procedure, each animal performed one trial where the platform was placed above the water to determine whether the vision of mice was normal. Animal with the visual problem would be excluded in the Morris water maze test. Each mouse was put into the pool to be trained and learned to search for the platform under the water in the order of quadrant II, III, IV and I with an inter-trial interval (ITI) of 60 min at almost the same time of each day for five days. The test was carried out without the platform on the fifth day, and each mouse was put into the pool at quadrant II and allowed for 60 seconds to track them.

Ex vivo verification

Western Blotting: The total protein in the brain tissue was extracted and the content of IL-1β, IL-6 and TNF-α was analyzed. SDS-PAGE electrophoresis was performed before transferring to the membrane. Immune responses of the specific antibodies were carried out and the images were captured with autoradiography. All antibodies were purchased from Abcam.

ELISA analysis: Inflammatory cytokines including IL-6, IL-1β and TNF-α were determined by ELISA kits (Abcam, ab100712, ab197742, ab208348, respectively), and the assays were performed as per the instructions provided by the manufacture.

Tissue staining: Brain tissues were taken out at 30 days post-injury and fixed in 4% paraformaldehyde and embedded in paraffin. Immunofluorescent staining was performed with primary antibodies including anti-GFAP, IL6, IL1β antibodies as per the instructions of (Abcam). Then the slices were incubated with Alexa Fluor 488/594-conjugated goat secondary antibody for 1-1.5 hours at room temperature under dark and counterstained with DAPI. Immunohistochemical staining for IL-6 and mice brain tissue was performed according to the instructions (Proteintech).

Abbreviations

TBI: Traumatic brain injury; ROS:reactive oxygen species; $OH^{\bullet}$:hydroxyl radical; $O_2^{\bullet-}$:superoxide anion radicals; H_2O_2:hydrogen peroxide; RNS:reactive nitrogen species; $NO^{\bullet}$:nitric oxide radicals; $ONOO^-$:peroxynitrite; RONS:reactive oxygen and nitrogen species; CAT:catalase; SOD:superoxide dismutase; POD:peroxidase; GPx:glutathione peroxidase; HER:hydrogen evolution reaction; OER:oxygen evolution reaction; DLS:dynamic light scattering; GC:glassy carbon; CV:Cyclic Voltammetry; LSV:Linear Sweep Voltammetry; ORR:Oxygen reduction reaction.

Declarations

Ethics approval and consent to participate

We have obtained approval of animal ethics and use committee (IRM-DWLL-2019099). All animal procedure was followed the guideline approved by the Institute of Radiation Medicine, Chinese Academy of Medical Sciences and Peking Union Medical College.

Consent for publication

All authors gave their consent for publication.

Availability of data and materials

The datasets used and analyzed during the current study are available from the corresponding author on reasonable request

Competing interests

The authors declare no conflict of interest.

Funding

This work was financially supported by the NSFC (Grant No. 91859101, 81971744, U1932107, and 81471786), the National Natural Science Foundation of Tianjin (19JCZDJC34000), the Foundation of ‘Peiyang Young Researcher’ Program of Tianjin University, and CAS Interdisciplinary Innovation Team (JCTD-2020-08).

Authors’ contributions

ZX, WH, and XJ originated the concept. ZY and SS wrote the manuscript. SS and LH worked on materials synthesis and characterizations. RQ, HW, and XQ worked on biological experiments. All authors read and approved the final manuscript.

Acknowledgements

Not applicable.

References

1. Simon DW, McGeachy MJ, Bayır H, Clark RS, Loane DJ, Kochanek PM. The far-reaching scope of neuroinflammation after traumatic brain injury. Nat Rev Neurol. 2017;13(3):171–91.
2. Jiang JY, Gao GY, Feng JF, Mao Q, Chen LG, Yang XF, Liu JF, Wang YH, Qiu BH, Huang XJ. Traumatic brain injury in China. Lancet Neurol. 2019;18(3):286–95.
3. Zhang XD, Wang H, Antaris AL, Li L, Diao S, Ma R, Nguyen A, Hong G, Ma Z, Wang J, et al. Traumatic brain injury imaging in the second near-infrared window with a molecular fluorophore. Adv Mater. 2016;28(32):6872–9.
4. Badhiwala JH, Wilson JR, Fehlings MG. Global burden of traumatic brain and spinal cord injury. Lancet Neurol. 2019;18(1):24–5.
5. James SL, Theadom A, Ellenbogen RG, Bannick MS, Montjoy-Venning W, Lucchesi LR, Abbasi N, Abdulkader R, Abraha HN, Adsuar JC. Global, regional, and national burden of traumatic brain injury and spinal cord injury, 1990–2016: a systematic analysis for the Global Burden of Disease Study 2016. Lancet Neurol. 2019;18(1):56–87.
6. Kolias AG, Rubiano AM, Figaji A, Servadei F, Hutchinson PJ. Traumatic brain injury: global collaboration for a global challenge. Lancet Neurol. 2019;18(2):136–37.
7. Khatri N, Thakur M, Pareek V, Kumar S, Sharma S, Datusalia AK. Oxidative stress: major threat in traumatic brain injury. CNS Neurol Disord Drug Targets. 2018;17(9):689–95.
8. Yoo D, Magsam AW, Kelly AM, Stayton PS, Kievit FM, Convertine AJ. Core-cross-linked nanoparticles reduce neuroinflammation and improve outcome in a mouse model of traumatic brain injury. ACS Nano. 2017;11(9):8600–11.
9. Yang B, Chen Y, Shi J. Nanocatalytic medicine. Adv Mater. 2019;31(39):1901778.
10. Jamjoom AAB, Rhodes J, Andrews PJD, Grant SGN. The synapse in traumatic brain injury. Brain. 2020;144(1):18–31.
11. Tarudji AW, Gee CC, Romereim SM, Convertine AJ, Kievit FM. Antioxidant thioether core-crosslinked nanoparticles prevent the bilateral spread of secondary injury to protect spatial learning and memory in a controlled cortical impact mouse model of traumatic brain injury. Biomaterials. 2021;272:120766.
12. Zhang S, Liu Y, Sun S, Wang J, Li Q, Yan R, Gao Y, Liu H, Liu S, Hao W, et al. Catalytic patch with redox Cr/CeO_2 nanozyme of noninvasive intervention for brain trauma. Theranostics. 2021;11(6):2806–21.
13. Mu X, He H, Wang J, Long W, Li Q, Liu H, Gao Y, Ouyang L, Ren Q, Sun S, et al. Carbogenic nanozyme with ultrahigh reactive nitrogen species selectivity for traumatic brain injury. Nano Lett. 2019;19(7):4527–34.
14. Mu X, Wang J, Li Y, Xu F, Long W, Ouyang L, Liu H, Jing Y, Wang J, Dai H, et al. Redox trimetallic nanozyme with neutral environment preference for brain injury. ACS Nano. 2019;13(2):1870–84.
15. Yan R, Sun S, Yang J, Long W, Wang J, Mu X, Li Q, Hao W, Zhang S, Liu H, et al. Nanozyme-based bandage with single-atom catalysis for brain trauma. ACS Nano. 2019;13(10):11552–60.

16. Wang Q, Jiang J, Gao L. Nanozyme-based medicine for enzymatic therapy: progress and challenges. Biomed Mater. 2021;16:042002.
17. Smith ES, Porterfield JE, Kannan RM. Leveraging the interplay of nanotechnology and neuroscience: Designing new avenues for treating central nervous system disorders. Adv Drug Deliv Rev. 2019;148:181–203.
18. Li Y, He X, Yin J-J, Ma Y, Zhang P, Li J, Ding Y, Zhang J, Zhao Y, Chai Z, et al. Acquired superoxide-scavenging ability of ceria nanoparticles. Angew Chem Int Ed. 2015;54(6):1832–35.
19. Tyo EC, Vajda S. Catalysis by clusters with precise numbers of atoms. Nat Nanotechnol. 2015;10(7):577–88.
20. Chen K, Sun S, Wang J, Zhang X-D. Catalytic nanozymes for central nervous system disease. Coord Chem Rev. 2021;432:213751.
21. Mendoza K, Derry PJ, Cherian LM, Garcia R, Nilewski L, Goodman JC, Mbye L, Robertson CS, Tour JM, Kent TA. Functional and Structural Improvement with a Catalytic Carbon Nano-Antioxidant in Experimental Traumatic Brain Injury Complicated by Hypotension and Resuscitation. J Neurotrauma. 2019;36(13):2139–46.
22. Wang X, He H, Wang Y, Wang J, Sun X, Xu H, Nau WM, Zhang X, Huang F. Active tumor-targeting luminescent gold clusters with efficient urinary excretion. Chem Commun. 2016;52(59):9232–5.
23. Li F, Li TY, Sun CX, Xia JH, Jiao Y, Xu HP. Selenium-doped carbon quantum dots for free-radical scavenging. Angew Chem Int Ed. 2017;56(33):9910–14.
24. Bharadwaj VN, Nguyen DT, Kodibagkar VD, Stabenfeldt SE. Nanoparticle-based therapeutics for brain injury. *Adv Healthc Mater.* 2018, 7(1).
25. Kim CK, Kim T, Choi IY, Soh M, Kim D, Kim YJ, Jang H, Yang HS, Kim JY, Park HK, et al. Ceria nanoparticles that can protect against ischemic stroke. Angew Chem Int Ed. 2012;51(44):11039–43.
26. Ghosh S, Roy P, Karmodak N, Jemmis ED, Mugesh G. Nanoisozymes: crystal-facet-dependent enzyme-mimetic activity of V_2O_5 nanomaterials. Angew Chem Int Ed. 2018;57(17):4510–15.
27. Montini T, Melchionna M, Monai M, Fornasiero P. Fundamentals and catalytic applications of CeO_2-based materials. Chem Rev. 2016;116(10):5987–6041.
28. Heckman KL, DeCoteau W, Estevez A, Reed KJ, Costanzo W, Sanford D, Leiter JC, Clauss J, Knapp K, Gomez C, et al. Custom cerium oxide nanoparticles protect against a free radical mediated autoimmune degenerative disease in the brain. ACS Nano. 2013;7(12):10582–96.
29. Liu H, Li Y, Sun S, Xin Q, Liu S, Mu X, Yuan X, Chen K, Wang H, Varga K, et al. Catalytically potent and selective clusterzymes for modulation of neuroinflammation through single-atom substitutions. Nat Commun. 2021;12(1):1–14.
30. Yuan SF, Lei Z, Guan ZJ, Wang QM. Atomically precise preorganization of open metal stes on gold nanoclusters with high catalytic performance. Angew Chem Int Ed. 2021;60(10):5225–29.
31. Higaki T, Li Y, Zhao S, Li Q, Li S, Du XS, Yang S, Chai J, Jin R. Atomically tailored gold nanoclusters for catalytic application. Angew Chem Int Ed. 2019;58(25):8291–302.

32. Tian S, Cao Y, Chen T, Zang S, Xie J. Ligand-protected atomically precise gold nanoclusters as model catalysts for oxidation reactions. Chem Commun. 2020;56(8):1163–74.
33. Sun S, Liu HL, Xin Q, Chen K, Ma HZ, Liu SH, Mu XY, Hao WT, Liu SJ, Gao YL, et al. Atomic engineering of clusterzyme for relieving acute neuroinflammation through lattice expansion. Nano Lett. 2021;21(6):2562–71.
34. Kudryashev JA, Waggoner LE, Leng HT, Mininni NH, Kwon EJ. An activity-based nanosensor for traumatic brain injury. ACS Sens. 2020;5(3):686–92.
35. Li C, Li W, Liu H, Zhang Y, Chen G, Li Z, Wang Q. An Aactivatable NIR-II nanoprobe for in vivo early real-time diagnosis of traumatic brain injury. Angew Chem Int Ed. 2020;59(1):247–52.
36. Li C, Shah KA, Narayan RK. Rapid detection of traumatic brain injury. Nat Biomed Eng. 2020;4(6):579–80.
37. Li Z, Ji S, Liu Y, Cao X, Tian S, Chen Y, Niu Z, Li Y. Well-defined materials for heterogeneous catalysis: from nanoparticles to isolated single-atom sites. Chem Rev. 2020;120(2):623–82.
38. Cai X, Saranya G, Shen KQ, Chen MY, Si R, Ding WP, Zhu Y. Reversible switching of catalytic activity by shuttling an atom into and out of gold nanoclusters. Angew Chem Int Ed. 2019;58(29):9964–68.
39. Kwak K, Lee D. Electrochemistry of atomically precise metal nanoclusters. Acc Chem Res. 2019;52(1):12–22.
40. Tang Q, Hu G, Fung V, Jiang DE. Insights into interfaces, stability, electronic properties, and catalytic activities of atomically precise metal nanoclusters from first principles. Acc Chem Res. 2018;51(11):2793–802.
41. Xu BL, Wang H, Wang WW, Gao LZ, Li SS, Pan XT, Wang HY, Yang HL, Meng XQ, Wu QW, et al. A single-atom nanozyme for wound disinfection applications. Angew Chem Int Ed. 2019;58(15):4911–16.
42. Zhang XD, Zhang J, Wang J, Yang J, Chen J, Shen X, Deng J, Deng D, Long W, Sun YM, et al. Highly catalytic nanodots with renal clearance for radiation protection. ACS Nano. 2016;10(4):4511–9.
43. Chen D, Li J. Ultrasmall au nanoclusters for bioanalytical and biomedical applications: the undisclosed and neglected roles of ligands in determining the nanoclusters' catalytic activities. Nanoscale Horiz. 2020;5(10):1355–67.
44. Zhou R, Yan L, Dong X, Zhu S, Chen K, Wu Y, Xiang H, Li L, Zhang G, Gu Z, et al. Fractionated regimen-suitable immunoradiotherapy sensitizer based on ultrasmall $Fe_4Se_2W_{18}$ nanoclusters enable tumor-specific radiosensitization augment and antitumor immunity boost. Nano Today. 2021;36(3):101003.
45. Joseph B, Khan M, Rhee P. Non-invasive diagnosis and treatment strategies for traumatic brain injury: an update. J Neurosci Res. 2018;96(4):589–600.
46. Strubakos CD, Malik M, Wider JM, Lee IS, Reynolds CA, Mitsias P, Przyklenk K, Huttemann M, Sanderson TH. Non-invasive treatment with near-infrared light: A novel mechanisms-based strategy that evokes sustained reduction in brain injury after stroke. J Cerebr Blood F Met. 2020;40(4):833–44.

47. Pink AE, Williams C, Alderman N, Stoffels M. The use of repetitive transcranial magnetic stimulation (rTMS) following traumatic brain injury (TBI): a scoping review. Neuropsychol Rehabil. 2021;31(3):479–505.
48. Gao G, Chen R, He M, Li J, Li J, Wang L, Sun T. Gold nanoclusters for Parkinson's disease treatment. Biomaterials. 2019;194:36–46.
49. Liu H, Hong G, Luo Z, Chen J, Chang J, Gong M, He H, Yang J, Yuan X, Li L, et al. Atomic-precision gold clusters for NIR-II imaging. Adv Mater. 2019;31(46):1901015.
50. Fan Y, Liu S, Yi Y, Rong H, Zhang J. Catalytic nanomaterials toward atomic levels for biomedical applications: from metal clusters to single-atom catalysts. ACS Nano. 2021;15(2):2005–37.
51. Zhu J, Cai L, Yin X, Wang Z, Zhang L, Ma H, Ke Y, Du Y, Xi S, Wee ATS, et al. Enhanced electrocatalytic hydrogen evolution activity in single-atom Pt-decorated VS_2 nanosheets. ACS Nano. 2020;14(5):5600–08.
52. Zhao S, Jin R, Abroshan H, Zeng C, Zhang H, House SD, Gottlieb E, Kim HJ, Yang JC, Jin R. Gold nanoclusters promote electrocatalytic water oxidation at the nanocluster/$CoSe_2$ interface. J Am Chem Soc. 2017;139(3):1077–80.
53. Wang JY, Mu X, Li Y, Xu F, Long W, Yang J, Bian P, Chen J, Ouyang L, Liu H, et al. Hollow PtPdRh nanocubes with enhanced catalytic activities for in vivo clearance of radiation-induced ROS via surface-mediated bond breaking. Small. 2018;14(13):e1703736.
54. Seong H, Efremov V, Park G, Kim H, Yoo JS, Lee D. Atomically precise gold nanoclusters as model catalysts for identifying active sites for electroreduction of CO_2. *Angew Chem Int Ed*. 2021.
55. Jiang Y, Zhao X, Huang J, Li J, Upputuri PK, Sun H, Han X, Pramanik M, Miao Y, Duan H, et al. Transformable hybrid semiconducting polymer nanozyme for second near-infrared photothermal ferrotherapy. Nat Commun. 2020;11(1):1857.
56. Fan K, Xi J, Fan L, Wang P, Zhu C, Tang Y, Xu X, Liang M, Jiang B, Yan X, et al. In vivo guiding nitrogen-doped carbon nanozyme for tumor catalytic therapy. Nat Commun. 2018;9(1):1440.
57. Yong Y, Zhang C, Gu Z, Du J, Guo Z, Dong X, Xie J, Zhang G, Liu X, Zhao Y. Polyoxometalate-based radiosensitization platform for treating hypoxic tumors by attenuating radioresistance and enhancing radiation response. ACS Nano. 2017;11(7):7164–76.
58. Ma M, Gao N, Li X, Liu Z, Pi Z, Du X, Ren J, Qu X. A biocompatible second near-infrared nanozyme for spatiotemporal and non-invasive attenuation of amyloid deposition through scalp and skull. ACS Nano. 2020;14(8):9894–903.
59. Wu H, Li F, Wang S, Lu J, Li J, Du Y, Sun X, Chen X, Gao J, Ling D. Ceria nanocrystals decorated mesoporous silica nanoparticle based ROS-scavenging tissue adhesive for highly efficient regenerative wound healing. Biomaterials. 2018;151:66–77.
60. Liu Y, Cheng Y, Zhang H, Zhou M, Yu Y, Lin S, Jiang B, Zhao X, Miao L, Wei CW, et al. Integrated cascade nanozyme catalyzes in vivo ROS scavenging for anti-inflammatory therapy. Sci Adv. 2020;6(29):eabb2695.

61. Yuan X, Goswami N, Mathews I, Yu Y, Xie JP. Enhancing stability through ligand-shell engineering: A case study with $Au_{25}(SR)_{18}$ nanoclusters. Nano Res. 2015;8(11):3488–95.
62. Yao Q, Chen T, Yuan X, Xie J. Toward total synthesis of thiolate-protected metal nanoclusters. Acc Chem Res. 2018;51(6):1338–48.
63. Vorhees CV, Williams MT. Morris water maze: procedures for assessing spatial and related forms of learning and memory. Nat Protoc. 2006;1(2):848–58.
64. D'Hooge R, De Deyn PP. Applications of the Morris water maze in the study of learning and memory. Brain Res Rev. 2001;36(1):60–90.

Figures

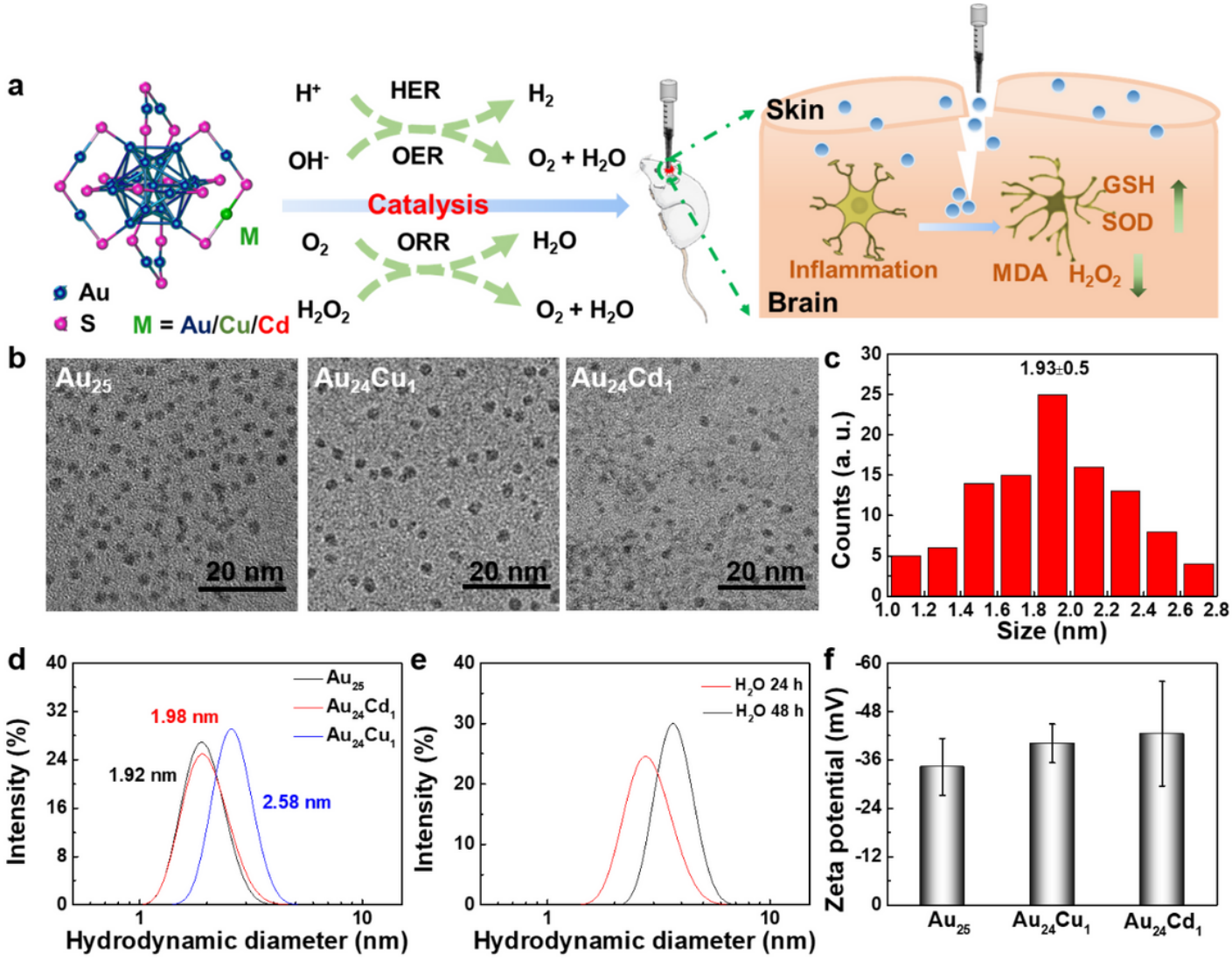

Figure 1

Structural characterization of Au25 nanoclusters. (a) Schematic illustration of noninvasive TBI treatment with gold nanoclusters via a catalytic system. (b) TEM image of MPA-protected Au25, Au24Cu1 and Au24Cd1 nanoclusters. Scale bar: 20 nm. (c) Size distribution of MPA-protected Au25 nanocluster

measured by analyzing 100 nanodots from TEM images. (d) Hydrodynamic diameters of MPA-protected Au25, Au24Cu1 and Au24Cd1 in PBS buffer, and the mean sizes of Au25, Au24Cu1 and Au24Cd1 were 1.98, 1.92 and 2.58 nm respectively. (e) Stability of Au25 nanocluster in H2O after 24 h and 48 h at room temperature, and the slightly increase of hydrodynamic diameter revealed satisfying stability. Additionally, the zeta potentials of the nanoclusters (f) were around -35 mV, indicative of good colloid stability (n=3 independent experiments, data are presented as mean ± SD).

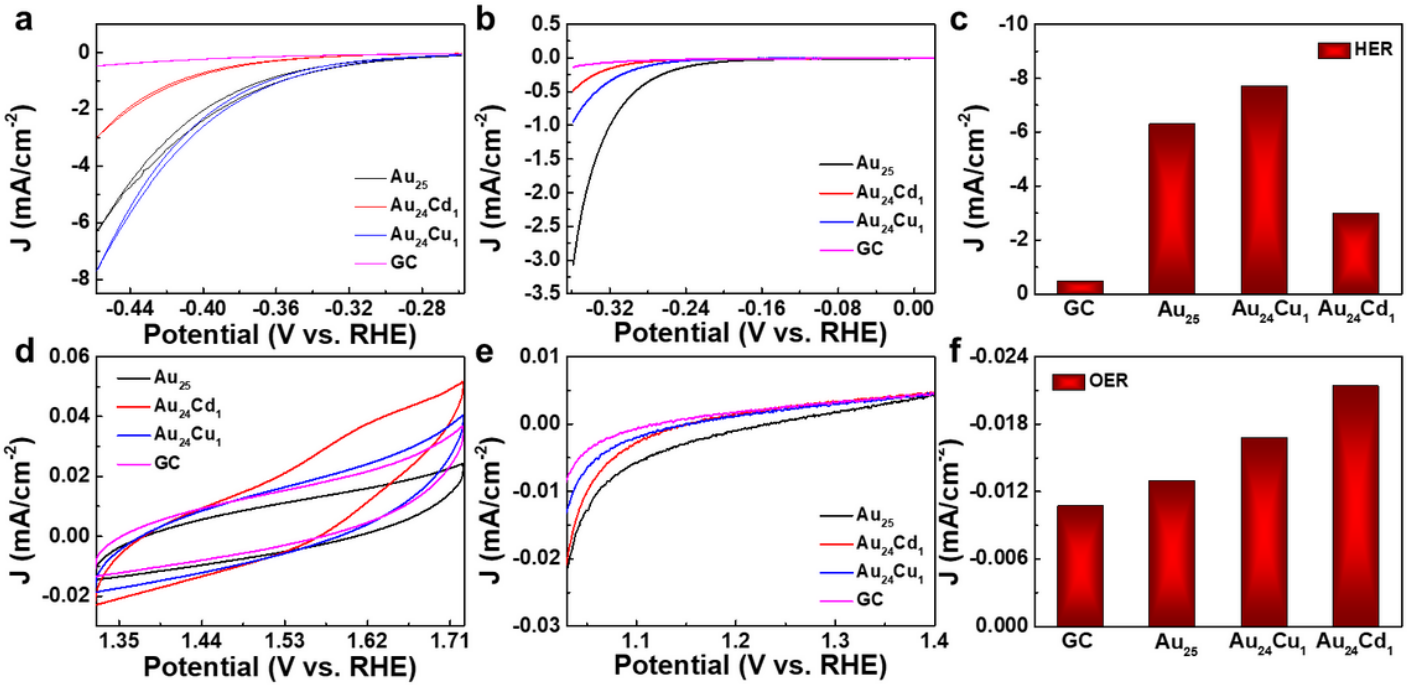

Figure 2

Catalytic performance for overall water splitting. (a) CVs of GC electrode modified with as-prepared Au25, Au24Cu1 and Au24Cd1 nanoclusters in 0.5 M H2SO4. (b) Linear sweep HER voltammograms for Au25, Au24Cu1 and Au24Cd1 nanoclusters. (c) Current density of different nanoclusters at the potential of −0.4585 V toward the activity of HER. (d) CVs of GC electrode modified with as-prepared Au25, Au24Cu1 and Au24Cd1 nanoclusters in 1 M KOH. (e) Linear sweep HER voltammograms for Au25, Au24Cu1 and Au24Cd1 nanoclusters. (f) Current density of different nanoclusters at the potential of 1.3244 V toward the activity of OER.

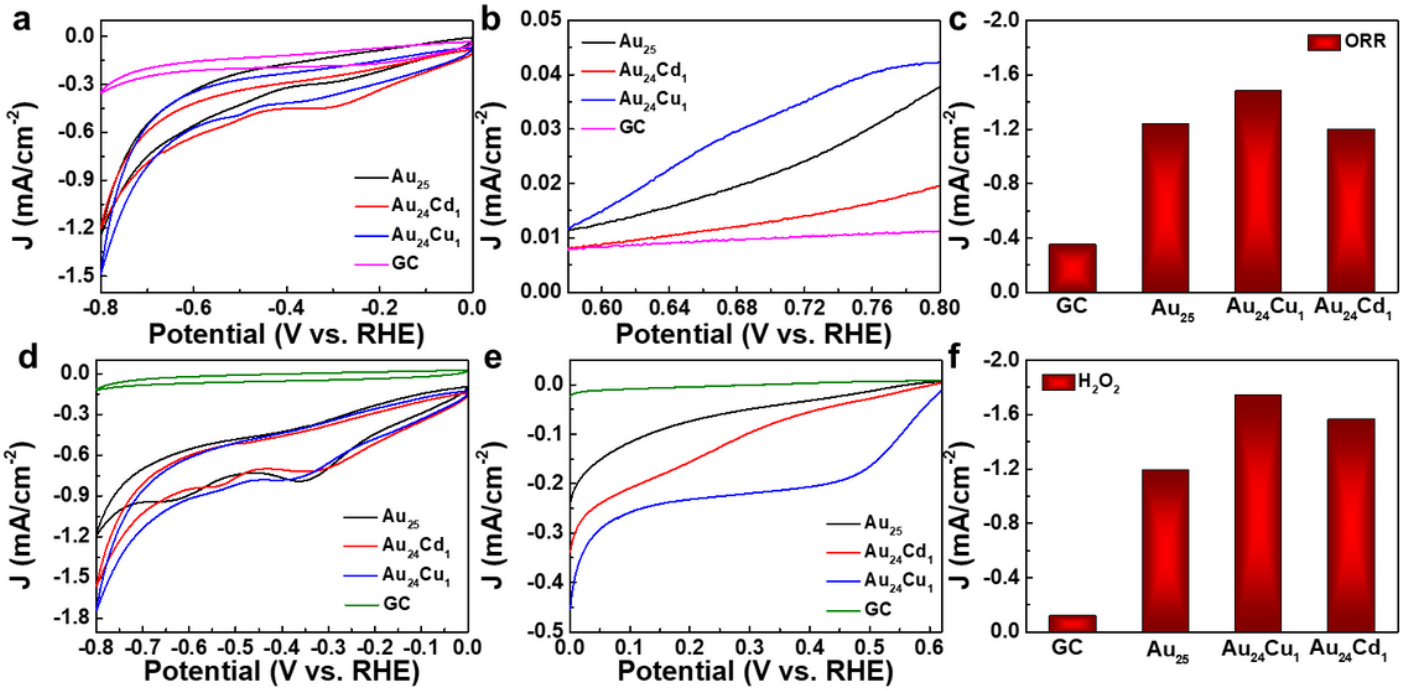

Figure 3

Catalytic activities of the Au25 nanoclusters. (a) CVs of GC electrode modified with as-prepared Au25, Au24Cu1 and Au24Cd1 nanoclusters in O2-saturated 0.01 M PBS (pH 7.4). (b) LSV of GC electrode modified with as-prepared Au25, Au24Cu1 and Au24Cd1 nanoclusters in O2-saturated 0.01 M PBS (pH 7.4). Scanning rate: 0.010 V s−1. Rotation rate: 1600 rpm. (c) Compared the ORR activities of Au25, Au24Cu1 and Au24Cd1 nanoclusters at the potential of −0.8 V. (d) CVs of GC electrode modified with as-prepared Au25, Au24Cu1 and Au24Cd1 nanoclusters in the presence of 9.8 mM H2O2 in N2-saturated 0.01 M PBS (pH 7.4). (e) LSV of GC electrode modified with as-prepared Au25, Au24Cu1 and Au24Cd1 nanoclusters in the presence of 9.8 mM H2O2 in N2-saturated 0.01 M PBS (pH 7.4). Scanning rate: 0.010 V s−1. Rotation rate: 1600 rpm. (f) Compared the H2O2 scavenging activities of nanoclusters at the potential of −0.8 V.

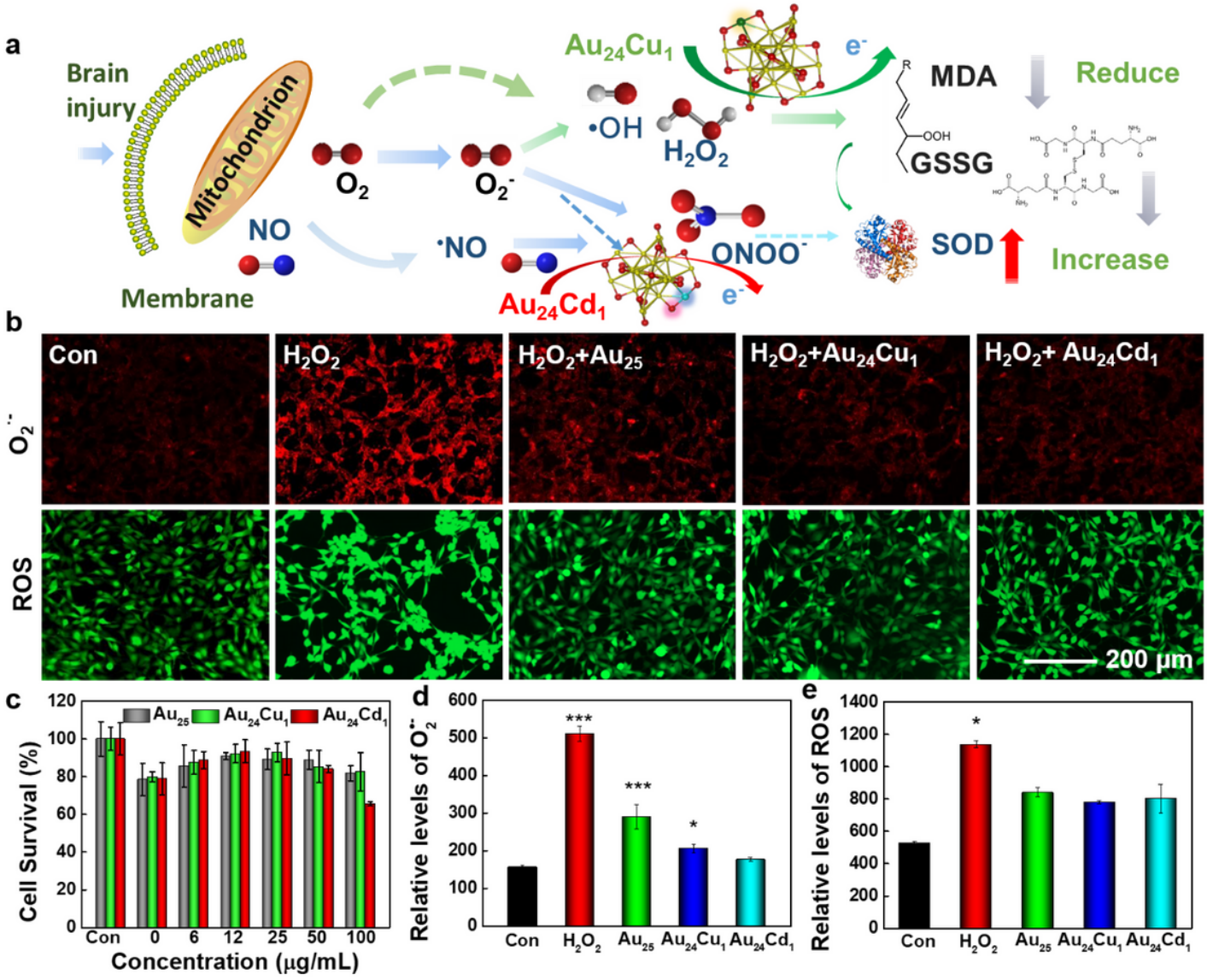

Figure 4

Catalytic mechanism and in vitro evaluation of the nanoclusters. (a) Schematic illustration of the catalytic mechanism and selectivity of the nanoclusters. Cu and Cd as single active sites exhibit superiorities against reactive oxygen species (ROS) and reactive nitrogen species (RNS) respectively, resulting in free radical scavenging and inspire their use in brain injury. (b) Fluorescence images of ROS (green) and O2•− (red) levels induced by 100 μM H2O2 with or without nanoclusters treatment, illustrating the high activity of scavenging ROS of the nanoclusters. (c) HT22 cell viability under treatment of H2O2 and treated with or without the nanoclusters (n = 5 per group, data are presented as mean ± SD), which showed the ability of the nanoclusters to rescue the lethality induce by H2O2. (d, e) Quantitative analysis of Au25, Au24Cu1 and Au24Cd1 against O2•− and ROS, respectively (n = 3 independent experiments, data are presented as mean ± SD).

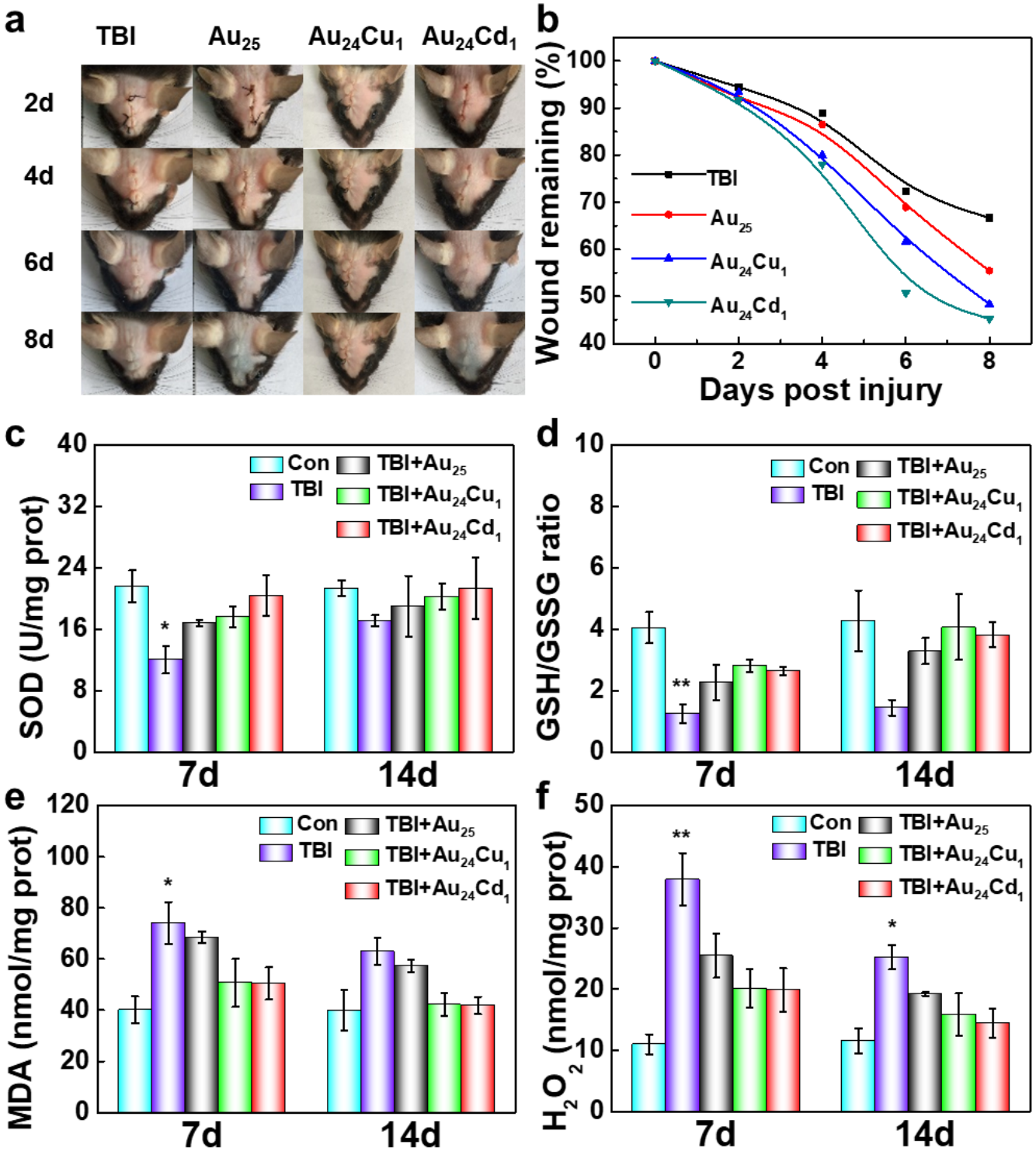

Figure 5

In vivo investigation of the nanoclusters. (a) Wound healing processes over time of TBI mice with and without treatment of nanoclusters, and (b) showed wound remaining percentage over time. The Au24Cu1 and Au24Cd1 showed favorable therapeutic effect against TBI. (c-f) Indicators for oxidative stress, including SOD, GSH/GSSG, MDA, and H2O2, of TBI mice with or without treatment of nanoclusters on days 7 and 14 post intervention (n = 3 per group). The nanoclusters can rescue the level of SOD and

GSH/GSSG decreased by TBI, and decrease the MDA and H2O2, indicative of alleviating the oxidative stress in vivo. Data are presented as mean ± SEM and compared with the Con groups, analyzed by one-way ANOVA with Turkey test (adjusted p values are shown).

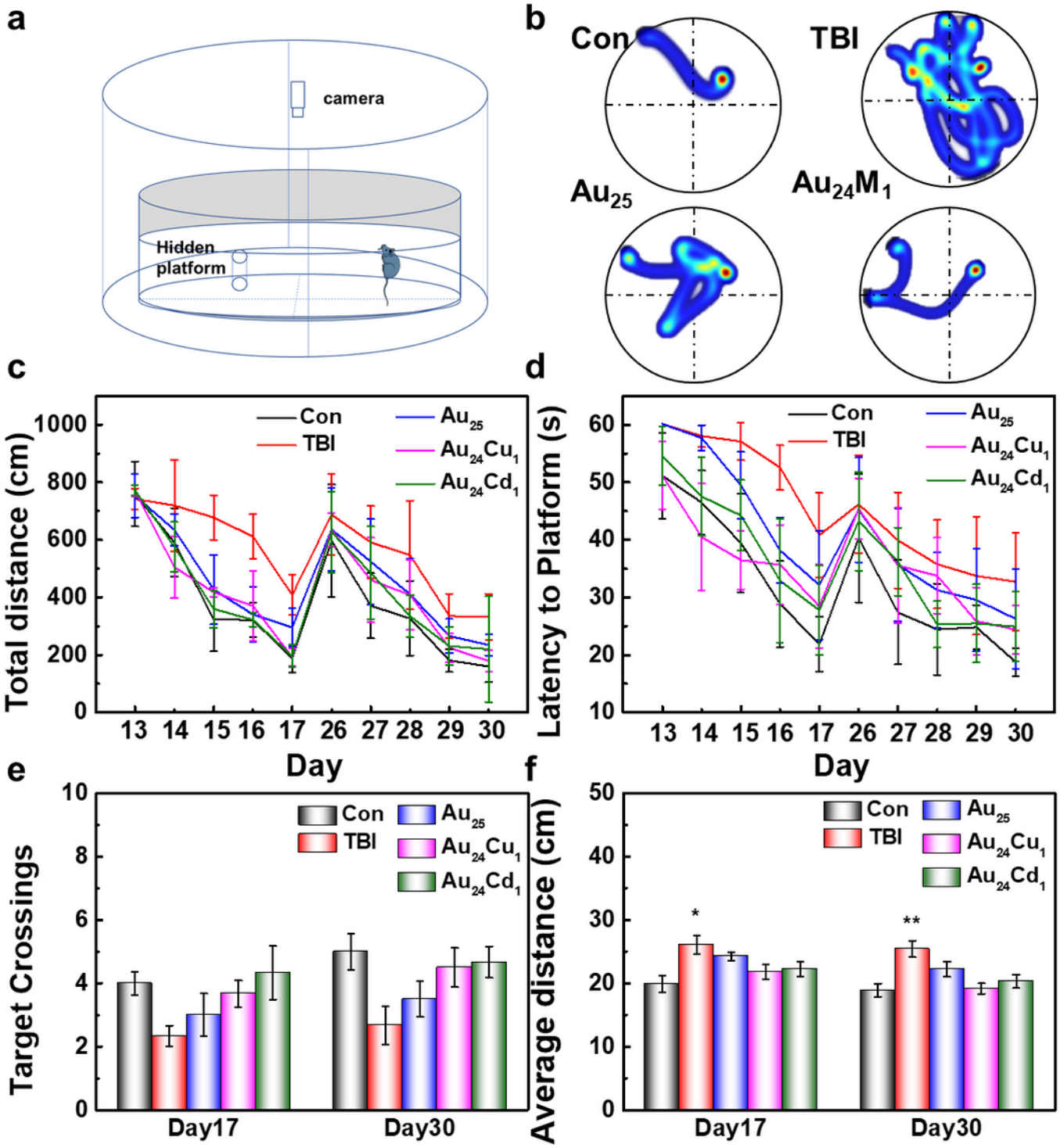

Figure 6

Morris water maze tests. (a) Schematic illustration of the apparatus. (b) Paths of tested mice to the platform treated with or without the nanoclusters. (c) Distance traveled to the hidden platform, and (d)

latency to locate and rest on the hidden platform of the tested mice on days 13-17 and 26-30. The number of platform crossings (e) and average distance to locate the platform of the tested mice recorded on day 17 and 30. Results illustrated that the nanoclusters especially the Au24Cu1 and Au24Cd1 promoting the recovery of neuronal cognition and the spatial learning and memory abilities of TBI mice. Data are presented as mean ± SEM and compared with the Con groups, analyzed by one-way ANOVA with Turkey test (adjusted p values are shown).

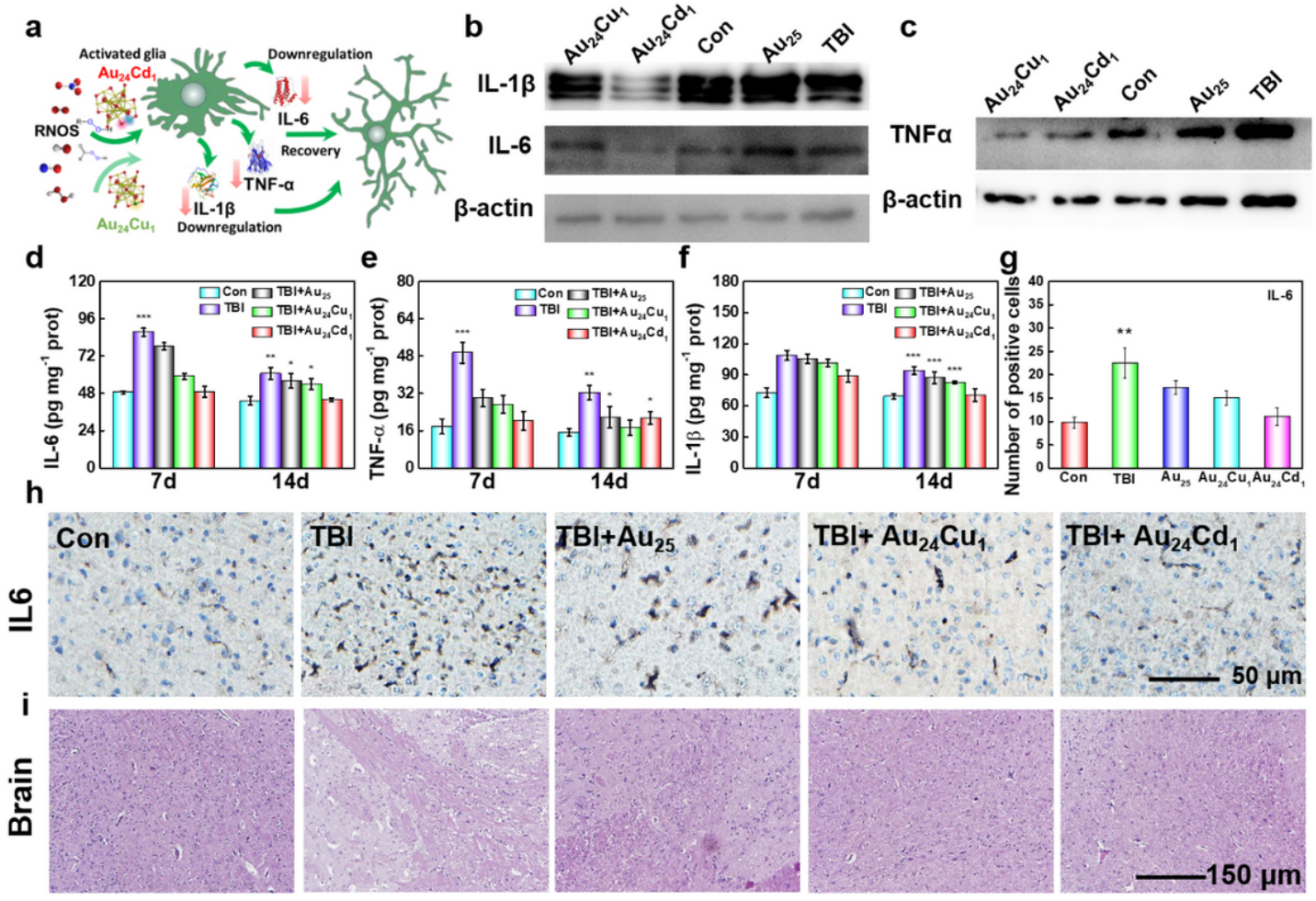

Figure 7

Inflammation levels in brain tissues. (a) Schematic illustration of catalytic activity on oxidative stress and inflammatory responses of the nanoclusters. Expression levels of IL-1β, IL-6 (b), and TNF-α (c) in the brain tissues on day 30 post TBI with or without nanoclusters (n =3 per group) were analyzed using western blotting. The Au24Cd1 showed superiority on downregulating the IL-1β and IL-6, while the Au24Cu1 had better effect toward TNF-α. (d-f) ELISA analysis of inflammatory factors on days 7 and 14 post TBI with or without treatment of nanoclusters (n = 3 per group) further confirmed the abilities of the Au24Cu1 and Au24Cd1 on regulating inflammatory factors. All the samples were derived from the same experiment and blots were processed in parallel. Data are presented as mean ± SEM and compared with the control

groups. (g) Quantitative analysis of the positive cell numbers in injured cortex with or without nanocluster treatment (n=3 per group). Analyzed by one-way ANOVA with Turkey test and compared with the Con groups. (h) The immunohistochemical assay illustrated the conspicuous effect of Au24Cd1 and Au24Cu1 aganst IL-6. (i) The pathological slices showed that the TBI group exhibiting apoptotic and swollen nerve cells and infiltration of inflammatory cells, while the groups treated with nanoclusters especially the Au24Cd1 and Au24Cu1 recovered to almost normal.

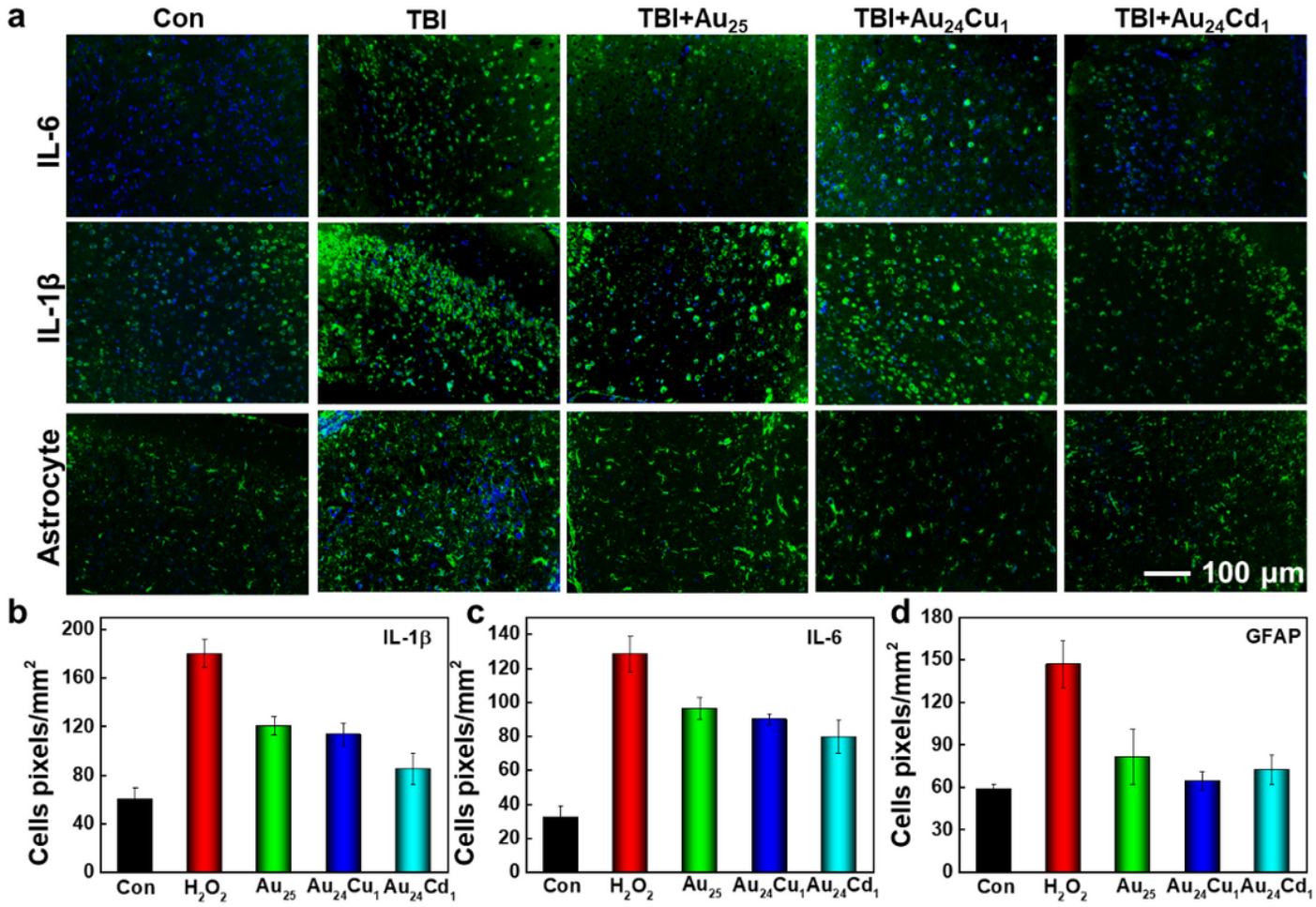

Figure 8

Staining characterization of inflammation levels. (a) Immunofluorescence staining of IL-6, IL-1β and astrocytes (GFAP) in injured cortex 30 days post TBI with or without nanocluster treatment. (b-d) Quantitative analysis of the expression of IL-6, IL-1β and GFAP with positive cells in the injured cortex with or without nanocluster treatment (n=3 per group). The Au24Cd1 and Au24Cu1 presented appealing effects of inhibiting the activation of astrocyte and the expression of IL-6 and IL-1β, which revealed excellent capability of the Au24Cd1 and Au24Cu1 on anti-neuroinflammation and further verified the effect of the nanoclusters against TBI.

Supplementary Files

This is a list of supplementary files associated with this preprint. Click to download.

- Graphicalabstracts.docx